



You have downloaded a document from
RE-BUŚ
repository of the University of Silesia in Katowice

Title: Symmetrical and unsymmetrical azomethines with thiophene core : structure - properties investigations

Author: Paweł Gnida, Agnieszka Pająk, Sonia Kotowicz, Jan Grzegorz Malecki, Mariola Siwy, Henryk Janeczek, Sebastian Maćkowski, Ewa Schab-Balcerzak

Citation style: Gnida Paweł, Pająk Agnieszka, Kotowicz Sonia, Malecki Jan Grzegorz, Siwy Mariola, Janeczek Henryk, Maćkowski Sebastian, Schab-Balcerzak Ewa. (2019). Symmetrical and unsymmetrical azomethines with thiophene core : structure - properties investigations. "Journal of Materials Science" (Vol. 54, iss. 21 (2019), s. 13491-13508), doi 10.1007/s10853-019-03853-6





Uznanie autorstwa - Licencja ta pozwala na kopiowanie, zmienianie, rozprowadzanie, przedstawianie i wykonywanie utworu jedynie pod warunkiem oznaczenia autorstwa.





Symmetrical and unsymmetrical azomethines with thiophene core: structure–properties investigations

Paweł Gnida¹ , Agnieszka Pająk² , Sonia Kotowicz² , Jan Grzegorz Malecki² ,
Mariola Siwy¹ , Henryk Janeczek¹ , Sebastian Maćkowski³ , and Ewa Schab-Balcerzak^{1,2,*} 

¹Centre of Polymer and Carbon Materials, Polish Academy of Sciences, 34 M. Curie-Skłodowska Str, 41-819 Zabrze, Poland

²Institute of Chemistry, University of Silesia, 9 Szkolna Str, 40-006 Katowice, Poland

³Institute of Physics, Faculty of Physics, Astronomy and Informatics, Nicolaus Copernicus University, 5 Grudziadzka Str, 87-100 Torun, Poland

Received: 7 May 2019

Accepted: 12 July 2019

Published online:

26 July 2019

© The Author(s) 2019

ABSTRACT

Unsymmetrical and symmetrical azomethines were obtained using the condensation reaction of diamino-thiophene-3,4 dicarboxylic acid diethyl ester with 4-(1-pyrrolidino)benzaldehyde, fluorene-2-carboxaldehyde, 1-methylindole-3-carboxaldehyde, and benzothiazole-2-carboxaldehyde. Their thermal, optical, and electrochemical properties were investigated, and the results were supported by calculations using the density functional theory. The studied compounds melted in the range of 170–260 °C and can be converted into amorphous materials with high glass transition temperatures between 76 and 135 °C. They were thermally stable up to 220–300 °C. All imines were electrochemically active and exhibited low energy band gaps below 2 eV (except for one imine with $E_g = 2.39$ eV) determined on the basis of cyclic voltammetry. Most of the azomethines were emissive in solution and in the solid state. Some of them showed both S_1 (first excited state) emission and S_2 (second excited state) emission or only fluorescence from higher excited state, which is first time observed for azomethines. The imine with the most promising properties was tested in a light-emitting diode, and its ability for emission of light under external voltage was demonstrated.

Address correspondence to E-mail: ewa.schab-balcerzak@us.edu.pl

Introduction

Nowadays, much attention is devoted to organic semiconductor materials for organic electronic applications, such as organic light-emitting diodes (OLEDs), organic photovoltaics (OPVs), flexible light displays, flat panel displays, sensors, nonlinear materials, or field effect transistors (FETs) [1, 2]. Organic compounds are characterized by many useful features, with the first perhaps being practically unlimited possibilities of chemical structure modifications for tuning their properties for particular applications and also the low cost of device production [1]. Among various small molecules synthesized for organic electronics, conjugated compounds containing imine bonds ($-\text{N}=\text{CH}-$) are known as Schiff bases or azomethines or imines. Imines are widely investigated not only for optoelectronics but also for medicine, pharmacy, synthesis, analysis, or catalysis [3]. Azomethines are an interesting alternative for typical conjugated materials because of their electron-withdrawing properties, high thermal and chemical stability, and synthesis advantages, such as mild reaction conditions, not requiring any expensive catalyst and with water being the only by-product; the purification process is also rather straightforward [2, 4–7]. Furthermore, the properties of this group of compounds can be rather easily modified by chemical doping of the imine bond [2]. Azomethines have been tested as components in photovoltaic cells [6, 8–10] and light-emitting diodes [5, 11–15]. Considering the influence of imines chemical structure on potential applications in organic electronics, it has been found that the most promising are heterocyclic azomethines and especially interesting seem to be imines with thiophene structure [16]. Compounds bearing thiophene units exhibit many features, like low band gap energy and low oxidation potentials, together with strong luminescence, thermal and chemical stability, as well as good electrical conductivity [17]. Azomethines with thiophene structure can be prepared from diamino-thiophene-3,4-dicarboxylic acid diethyl ester (DAT) and various aldehydes [16]. Encouraged by the results presented in Skene et al. [18] and in our work [19], we synthesized a series of symmetrical azomethines as well as comparable unsymmetrical ones, end-capped with the amine group. It is expected that the presence of the amine group in unsymmetrical imines can allow

hydrogen bond formation for enhancing fluorescence [18]. In this paper, the relationship between chemical structures of the substituent attached to imine bonds and potential application properties are presented. The thermal (TGA, DSC), optical (UV-Vis, PL), and electrochemical (CV) properties, together with the possibility of production of light under applied external voltage, were evaluated. Moreover, using density functional theory (DFT) electronic structure, photophysical properties and possibility of hydrogen bond formation were calculated.

Experimental section

Materials

Aldehydes (4-(1-pyrrolidino)benzaldehyde, fluorene-2-carboxaldehyde, 1-methylindole-3-carboxaldehyde, benzothiazole-2-carboxaldehyde), hexane, *N,N*-dimethylacetamide (DMA), dimethylformamide (DMF), *N*-methyl-pyrrolidone (NMP), sulfur, ethyl cyanoacetate, and triethylamine were purchased from Sigma-Aldrich. 2,5-Diamino-thiophene-3,4-dicarboxylic acid diethyl ester (DAT) was synthesized according to publication [20].

Azomethines synthesis

The azomethines were synthesized using melt condensation. An aldehyde (0.5 mmol) (4-(1-pyrrolidino)benzaldehyde at 85 °C, fluorene-2-carboxaldehyde at 84 °C, 1-methylindole-3-carboxaldehyde at 68 °C and benzothiazole-2-carboxaldehyde at 77 °C under argon atmosphere was melted, then DAT (0.25 mmol) and DMA (200 μL) was added. The reaction mixture was stirred for 24 h (unsymmetrical azomethines—**AzTh-1a**, **AzTh-2a**, **AzTh-3a**, **AzTh-4a**) or 35 h (symmetrical azomethines—**AzTh-1b**, **AzTh-2b**, **AzTh-3b**, **AzTh-4b**). The product was dissolved in chloroform and precipitated in hexane. Then the product was washed several times with hexane and dried at 40 °C in a vacuum oven for 24 h.

AzTh-1a: Dark brown solid. Yield = 79%, $^1\text{H NMR}$ (400 MHz, $\text{DMSO}-d_6$, δ , ppm): 7.90 (s, 1H, $\text{HC}=\text{N}$), 7.72 (s, 2H, NH_2), 7.58 (d, $J = 8.8$ Hz, 2H, CH), 6.59 (d, $J = 8.8$ Hz, 2H, CH), 4.25 (q, $J = 7.4$ Hz, 2H, $\text{O}-\text{CH}_2-$), 4.13 (q, $J = 7.2$ Hz, 2H, $\text{O}-\text{CH}_2-$), 1.97 (s, 4H, CH_2), 1.30 (t, $J = 7.0$ Hz, 3H, CH_3), 1.20 (t,

$J = 7.1$ Hz, 3H, CH₃). ¹³C NMR (101 MHz, DMSO-*d*₆, δ , ppm): 165.60, 163.91, 160.24, 153.40, 149.98, 134.25, 130.33, 126.81, 123.19, 112.06, 100.22, 60.99, 59.79, 47.79, 25.41, 14.65, 14, 59. ¹H NMR (400 MHz, CDCl₃, δ , ppm): 7.90 (s, 1H, HC=N), 7.64 (d, $J = 8.6$ Hz, 2H, CH), 7.28 (s, 1H, CH), 6.57 (d, $J = 8.6$ Hz, 2H, CH), 6.21 (s, 2H, NH₂), 4.42 (q, $J = 7.1$ Hz, 2H, O-CH₂-), 4.26 (q, $J = 7.1$ Hz, 2H, O-CH₂-), 3.38 (s, 4H, CH₂), 2.05 (s, 4H, CH₂), 1.45 (t, $J = 7.1$ Hz, 3H), 1.33 (t, $J = 7.1$ Hz, 3H). ¹³C NMR (400 MHz, CDCl₃, δ , ppm): The product was insufficiently soluble for analysis. FTIR (KBr, ν , cm⁻¹): 3388, 3305 (NH₂ stretch), 3071 (C-H aromatic), 2980, 2856 (C-H aliphatic), 1727 (C=O), 1674 (CH=N stretch), 1251 (C-N stretch). Anal. Calcd for C₂₁H₂₅N₃O₄S (415.51 g mol⁻¹): C, 60.70; H, 6.06; N, 10.11; Found: C, 60.52; H, 6.19; N, 10.08.

AzTh-1b: Dark brown solid. Yield = 55%, ¹H NMR (400 MHz, DMSO-*d*₆, δ , ppm): 8.32 (s, 2H, HC=N), 7.73 (d, $J = 8.8$ Hz, 4H, CH), 6.66 (d, $J = 8.8$ Hz, 4H, CH), 4.25 (q, $J = 7.1$ Hz, 4H, O-CH₂-), 3.37 (m, 4H, CH₂), 1.98 (m, 4H, CH₂), 1.29 (t, $J = 7.0$ Hz, 6H, CH₃). ¹³C NMR (101 MHz, DMSO-*d*₆, δ , ppm): 163.49, 159.52, 151.03, 131.74, 130.32, 124.56, 122.62, 112.22, 60.97, 47.86, 31.08, 25.38, 14.54. FTIR (KBr, ν , cm⁻¹): 3076 (C-H aromatic), 2965, 2837 (C-H aliphatic), 1733 (C=O), 1686 (CH=N stretch), 1245 (C-N stretch). Anal. Calcd for C₃₂H₃₆N₄O₄S (572.72 g mol⁻¹): C, 67.11; H, 6.34; N, 9.78; Found: C, 67.27; H, 6.22; N, 9.64.

AzTh-2a: Dark yellow solid. Yield = 35%, ¹H NMR (400 MHz, DMSO-*d*₆, δ , ppm): 8.17 (s, 1H, -HC=N-), 7.98 (t, $J = 8.5$ Hz, 2H, -CH), 7.95 (s, 1H, -CH), 7.92 (s, 2H, -NH₂), 7.81 (d, $J = 7.9$ Hz, 1H, -CH), 7.62 (d, $J = 7.0$ Hz, 1H, -CH), 7.46-7.33 (m, 2H, -CH), 4.31 (q, $J = 6.9$ Hz, 2H, -O-CH₂-), 4.16 (q, $J = 7.2$ Hz, 2H, -O-CH₂-), 4.00 (s, 2H, -CH₂), 1.35 (t, $J = 7.0$ Hz, 3H, -CH₃), 1.21 (t, $J = 7.0$ Hz, 3H, -CH₃). ¹³C NMR (101 MHz, DMSO-*d*₆, δ , ppm): The product was insufficiently soluble for analysis. ¹H NMR (400 MHz, CDCl₃, δ , ppm): 8.05 (s, 1H, HC=N), 7.97 (s, 1H, CH), 7.81 (dd, $J = 7.2, 6.2$ Hz, 2H, CH), 7.75 (d, $J = 7.9$ Hz, 1H, CH), 7.58 (d, $J = 7.3$ Hz, 1H, CH), 7.44-7.33 (m, 2H), 6.36 (s, 2H, NH₂), 4.48 (q, $J = 7.1$ Hz, 2H, O-CH₂-), 4.28 (q, $J = 7.2$ Hz, 2H, O-CH₂-), 3.94 (s, 2H, CH₂), 1.48 (t, $J = 7.2$ Hz, 3H, CH₃), 1.35 (t, $J = 7.0$ Hz, 3H, CH₃). ¹³C NMR (101 MHz, CDCl₃, δ , ppm): 165.63, 164.48, 159.52, 153.31, 144.66, 144.15, 143.57, 140.99, 134.82, 134.45, 129.20, 128.16, 127.52, 126.97, 125.17, 124.64, 120.50, 119.95, 103.16,

61.51, 60.27, 36.79, 14.38, 14.23. FTIR (KBr, ν , cm⁻¹): 3443, 3335 (NH₂ stretch), 3052 (C-H aromatic), 2982, 2907 (C-H aliphatic), 1729 (C=O), 1674 (CH=N stretch), 1254 (C-N stretch). Anal. Calcd for C₂₄H₂₂N₂O₄S (434.51 g mol⁻¹): C, 66.34; H, 5.10; N, 6.45; Found: C, 65.94; H, 5.01; N, 6.13.

AzTh-2b: Dark red solid. Yield = 22%, ¹H NMR (400 MHz, DMSO-*d*₆, δ , ppm): 8.70 (s, 2H, HC=N), 8.17 (s, 2H, CH), 8.07 (d, $J = 7.8$ Hz, 2H, CH), 8.00 (t, $J = 7.0$ Hz, 4H, CH), 7.66 (d, $J = 7.0$ Hz, 2H, CH), 7.52-7.33 (m, 4H, CH), 4.33 (q, $J = 7.1$ Hz, 4H, O-CH₂-), 4.05 (s, 4H, CH₂), 1.34 (t, $J = 7.0$ Hz, 6H, CH₃). Lit. [2]. ¹³C NMR (101 MHz, DMSO-*d*₆, δ , ppm): 163.01, 161.33, 149.94, 145.94, 144.78, 144.16, 140.66, 134.20, 129.45, 128.47, 127.52, 126.62, 125.97, 125.79, 121.43, 120.91, 61.38, 36.85, 14.53. FTIR (KBr, ν , cm⁻¹): 3050 (C-H aromatic), 2976, 2899 (C-H aliphatic), 1732 (C=O), 1687 (CH=N stretch), 1249 (C-N stretch). Anal. Calcd for C₃₈H₃₀N₂O₄S (610.72 g mol⁻¹): C, 74.73; H, 4.95; N, 4.59; Found: C, 73.87; H, 4.52; N, 4.57.

AzTh-3a: Dark red solid. Yield = 32%, ¹H NMR (400 MHz, DMSO-*d*₆, δ , ppm): 8.23 (d, $J = 6.4$ Hz, 2H, HC=N, CH), 7.92 (s, 1H, CH), 7.69 (s, 2H, NH₂), 7.52 (d, $J = 8.2$ Hz, 1H, CH), 7.31-7.25 (m, 1H, CH), 7.20-7.14 (m, 1H, CH), 4.31 (q, $J = 7.1$ Hz, 2H, O-CH₂-), 4.14 (q, $J = 7.1$ Hz, 2H, O-CH₂-), 3.86 (s, 3H, N-CH₃), 1.35 (t, $J = 7.1$ Hz, 3H, CH₃), 1.22 (t, $J = 7.1$ Hz, 3H, CH₃). ¹³C NMR (101 MHz, DMSO-*d*₆, δ , ppm): 165.00, 163.88, 159.67, 148.66, 138.05, 136.61, 134.83, 126.14, 125.44, 123.53, 122.40, 121.56, 114.01, 110.94, 100.16, 61.19, 59.80, 34.95, 33.50, 14.61, 14.58. FTIR (KBr, ν , cm⁻¹): 3428, 3316 (NH₂ stretch), 3052 (C-H aromatic), 2974, 2836 (C-H aliphatic), 1713 (C=O), 1675 (CH=N stretch), 1257 (C-N stretch). Anal. Calcd for C₂₀H₂₁N₃O₄S (399.46 g mol⁻¹): C, 60.13; H, 5.30; N, 10.52; Found: C, 60.52; H, 5.41; N, 10.32.

AzTh-3b: Dark red solid. Yield = 39%, ¹H NMR (400 MHz, DMSO-*d*₆, δ , ppm): 8.67 (s, 2H, HC=N), 8.43 (d, $J = 7.7$ Hz, 2H, CH), 8.13 (s, 2H, CH), 7.59 (d, $J = 8.2$ Hz, 2H, CH), 7.38-7.31 (m, 2H, CH), 7.30-7.23 (m, 2H, CH), 4.33 (q, $J = 7.1$ Hz, 4H, O-CH₂-), 3.91 (s, 6H, N-CH₃), 1.35 (t, $J = 7.1$ Hz, 6H, CH₃). ¹³C NMR (101 MHz, DMSO-*d*₆, δ , ppm): 163.81, 154.20, 150.09, 139.45, 138.49, 125.57, 124.55, 123.98, 122.76, 122.29, 114.12, 111.24, 61.22, 33.75, 31.16, 14.54. FTIR (KBr, ν , cm⁻¹): 3053 (C-H aromatic), 2978, 2837 (C-H aliphatic), 1716 (C=O), 1645 (CH=N stretch), 1256 (C-N stretch). Anal. Calcd for C₃₀H₂₈N₄O₄S

(540.63 g mol⁻¹): C, 66.65; H, 5.22; N, 10.36; Found: C, 66.19; H, 5.11; N, 10.38.

AzTh-4a: Dark orange solid. Yield = 29%, ¹H NMR (400 MHz, DMSO-*d*₆, δ, ppm): 8.26 (s, 1H, HC=N), 8.24 (s, 2H, NH₂), 8.14 (d, *J* = 7.3 Hz, 1H, CH), 8.05 (d, *J* = 7.7 Hz, 1H, CH), 7.60–7.46 (m, 2H, CH), 4.33 (q, *J* = 7.1 Hz, 2H, O–CH₂–), 4.17 (q, *J* = 7.1 Hz, 2H, O–CH₂–), 1.37 (t, *J* = 7.1 Hz, 3H, CH₃), 1.23 (t, *J* = 7.1 Hz, 3H, CH₃). ¹³C NMR (101 MHz, DMSO-*d*₆, δ, ppm): The product was insufficiently soluble for analysis. ¹H NMR (400 MHz, CDCl₃, δ, ppm): 8.72 (s, H, HC=N), 8.11 (d, *J* = 7.9 Hz, 1H, CH), 8.04 (d, *J* = 8.1 Hz, 1H, CH), 7.56–7.45 (m, 2H, CH), 6.65 (s, 2H, NH₂), 4.54 (q, *J* = 7.1 Hz, 2H, O–CH₂–), 4.28 (q, *J* = 7.0 Hz, 2H, O–CH₂–), 1.54 (t, *J* = 7.1 Hz, 3H, CH₃), 1.34 (t, *J* = 7.1 Hz, 3 H, CH₃). ¹³C NMR (101 MHz, CDCl₃, δ, ppm): The product was insufficiently soluble for analysis. FTIR (KBr, *v*, cm⁻¹): 3394, 3238(NH₂ stretch), 3059 (C–H aromatic), 2978, 2932 (C–H aliphatic), 1735 (C=O), 1676 (CH=N stretch), 1243 (C–N stretch). **Anal. Calcd** for C₁₈H₁₇N₃O₄S₂ (403.47 g mol⁻¹): C, 53.58; H, 4.25; N, 10.41; Found: C, 53.22; H, 4.17; N, 10.01.

AzTh-4b: Red solid. Yield = 50%, ¹H NMR (400 MHz, CDCl₃, δ, ppm): δ 8.76 (s, 2H, HC=N), 8.26 (d, *J* = 8.0 Hz, 2H, CH), 8.14 (d, *J* = 8.0 Hz, 2H, CH), 7.61–7.45 (m, 4H, CH), 4.54 (t, *J* = 7.1 Hz, 4H, O–CH₂–), 1.50 (t, *J* = 7.1 Hz, 6H, CH₃). ¹³C NMR (101 MHz, CDCl₃, δ, ppm): 167.86, 166.43, 164.76, 163.71, 154.15, 153.26, 150.18, 146.33, 139.50, 138.68, 135.80, 130.99, 129.92, 127.32, 126.67, 125.67, 124.45, 122.67, 121.96, 114.78, 62.09, 14.56, 14.12. FTIR (KBr, *v*, cm⁻¹): 3060 (C–H aromatic), 2985, 2898 (C–H aliphatic), 1748 (C=O), 1686 (CH=N stretch), 1233 (C–N stretch). **Anal. Calcd** for C₂₆H₂₀N₄O₄S₃ (548.66 g mol⁻¹): C, 56.92; H, 3.67; N, 10.21; Found: C, 56.91; H, 4.07; N, 10.45.

Results and discussion

A series of imines was prepared by condensing diamino-thiophene-3,4-dicarboxylic acid diethyl ester (DAT) with (4-(1-pyrrolidino)benzaldehyde, fluorene-2-carboxaldehyde, 1-methylindole-3-carboxaldehyde, and benzothiazole-2-carboxaldehyde. Utilization of different reaction times, 24 or 35 h, allowed to obtain unsymmetrical and symmetrical azomethines, respectively. All synthesized compounds, except for the one obtained by using

fluorene-2-carboxaldehyde, are new. The mentioned symmetrical azomethine with fluorene substituents has been presented by Skene et al. [21]. However, this imine has been prepared in different reaction conditions and its thermal and photophysical properties in the solid state together with the ability to show electroluminescence have not been yet reported.

Structural characterization of targeted imines

Chemical structures of the synthesized symmetrical and unsymmetrical azomethines are depicted in Fig. 1. Additionally, the photographs of prepared compounds in the solid state under daylight and UV irradiation are presented in the Supplementary Material in Table S1.

The chemical structure of obtained azomethines was confirmed by instrumental techniques, such as NMR, FTIR, and elemental analysis. In the ¹H NMR spectra of investigated imines, the signal of the imine proton (–HC=N–) was observed in the range of 7.90–8.76 ppm. In the case of symmetrical compounds, it was seen above 8.30 ppm and was shifted toward the lower field in comparison with unsymmetrical molecules. The signal of the proton in the aldehyde group (–COH) was not observed, which confirms the condensation reaction. Considering unsymmetrical azomethines, the characteristic signals for the protons in amine group were recorded from 6.21 ppm (**AzTh-1a** in CDCl₃) to 8.24 ppm (**AzTh-4a** in DMSO-*d*₆), which are absent in spectra measured for symmetrical compounds. The signal of protons coming from aliphatic methylene (–CH₂) group was found at 1.97 ppm for unsymmetrical **AzTh-1a** in DMSO-*d*₆, and however, separate two signals were found in the CDCl₃ at 3.38 and 2.05 ppm. For symmetrical **AzTh-1b**, such signals were found at 3.37 and 1.98 ppm in DMSO-*d*₆. The signals of –CH₂ group at about 4.00 ppm for unsymmetrical and symmetrical **AzTh-2a** were also seen. The signals of a methyl group (–N–CH₃) belonging to **AzTh-3a** and **AzTh-3b** were seen as a singlet at 3.86 ppm and at 3.91 ppm, respectively. Moreover, in ¹³C NMR spectra, the signals in the range of 163.01–167.86 ppm confirmed the presence of carbon atoms belonging to the –HC=N– bonds. In FTIR spectra, a characteristic absorption band of azomethine linkages from 1645 cm⁻¹ (**AzTh-3b**) to 1687 cm⁻¹ (**AzTh-2b**) was detected. The absorption

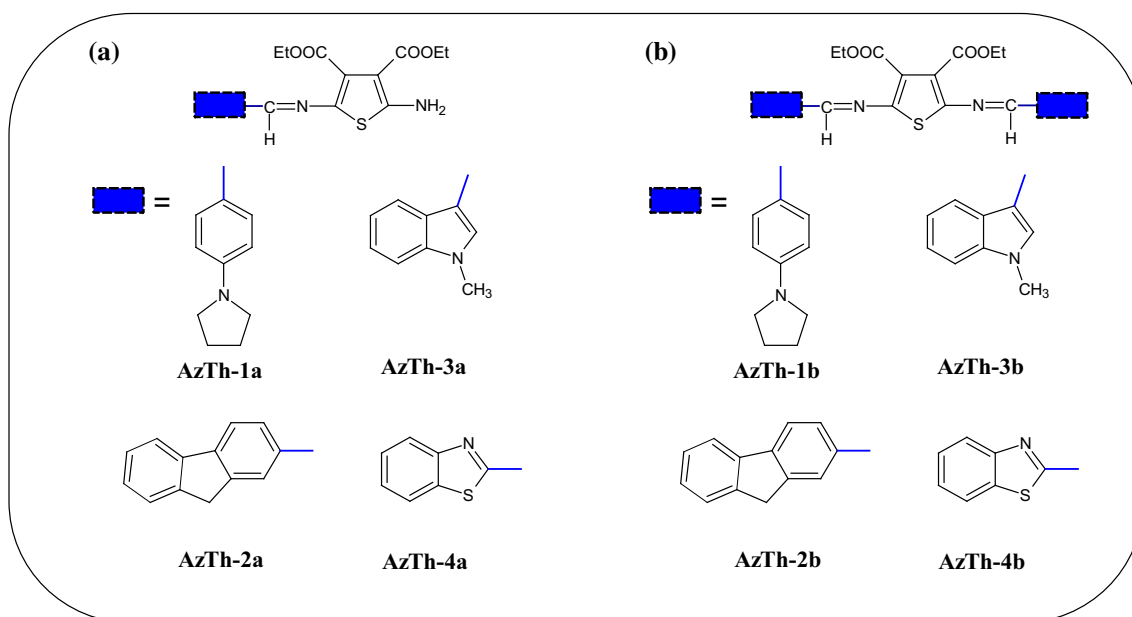


Figure 1 The chemical structure of the synthesized **a** unsymmetrical and **b** symmetrical thiophene azomethines.

bands due to aromatic and aliphatic groups were seen in the typical ranges, that is, $3076\text{--}3050\text{ cm}^{-1}$ and $2985\text{--}2836\text{ cm}^{-1}$, respectively. Additionally, for unsymmetrical azomethines, two absorption bands at $3385\text{--}3443\text{ cm}^{-1}$ and $3238\text{--}3335\text{ cm}^{-1}$ characteristic for --NH_2 were detected. The carbonyl absorption bands in the ester group (--C=O) in the range of $1713\text{--}1748\text{ cm}^{-1}$ were recorded. The elemental analysis results confirmed the chemical structure of the obtained compounds. The studied imines are soluble in typical organic solvents except for **AzTh-4b**, which was insoluble in DMSO. Synthesized compounds were received as powders with different colors depending on substituent structure (cf. Table S1).

Hydrogen bond formation: theoretical and experimental approaches

It was found that primary end-amine groups in imines can form hydrogen bonds, which may enhance fluorescence [18]. The hydrogen bonds may occur between the hydrogen atom and more electroactive atoms, and thus, in the case of synthesized unsymmetrical azomethines, they can appear between the ester and the amine groups. In the beginning, the possibility of H-bonds formation was evaluated using the density functional theory calculations (DFT). Based on the optimized geometries, the presence of the intramolecular hydrogen bonds between --NH_2

proton and an oxygen atom from ester group in the unsymmetrical azomethines was analyzed (cf. Fig. S1 in Supplementary Material). In the hydrogen bond are involved carbonyl C=O , in the case of **AzTh-1a** and **AzTh-4a**, and ester $\text{C--O--C}_2\text{H}_5$, in **AzTh-2a**, **AzTh-3a**, oxygen atoms. The calculated $\text{C=O}\cdots\text{H--N}$ distances in the case of the studied unsymmetrical azomethines in the range from 1.96 to 2.04 \AA are in line with the experimental value equal to 2.04 \AA determined for ethyl 2-amino-4-phenylthiophene-3-carboxylate [22]. The carbonyl oxygen in **AzTh-1a** and **AzTh-4a** is more electronegative compared to the ester one, while in the **AzTh-2a** and **AzTh-3a** molecules the calculated natural charges on both oxygen atoms are almost same (cf. Fig. S3 and Table S2). The energy of hydrogen bond between amine proton and carbonyl oxygen is higher compared to the one, in which the oxygen from ester bond takes part, as can be seen from the potential energy curves shown in Fig. 2 and Fig. S4 in Supplementary material.

The existence of hydrogen bonds was experimentally confirmed using ^1H NMR spectroscopy. The ^1H NMR spectra of unsymmetrical azomethines at different temperatures are presented in Fig. 3.

The protons of the amine group of **AzTh-1a**–**AzTh-4a** at room temperature ($25\text{ }^\circ\text{C}$) were seen at 7.72 ppm, 7.92 ppm, 7.69 ppm, and 8.24 ppm, whereas at $60\text{ }^\circ\text{C}$ the chemical shift to lower

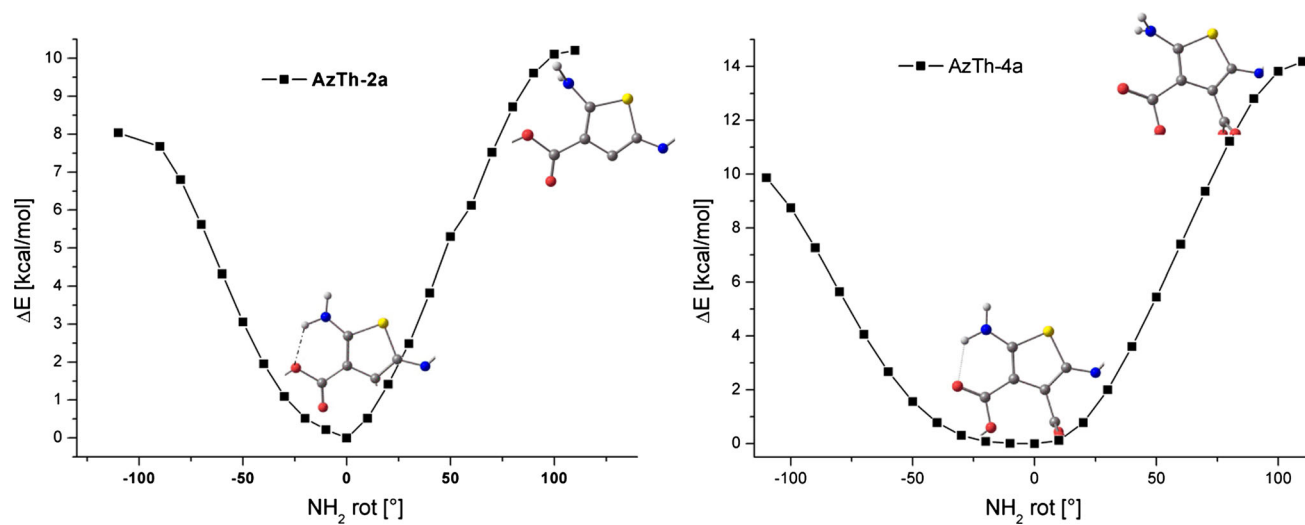


Figure 2 Potential energy profiles along the rotation of -NH_2 group in **AzTh-2a** and **AzTh-4a** molecules.

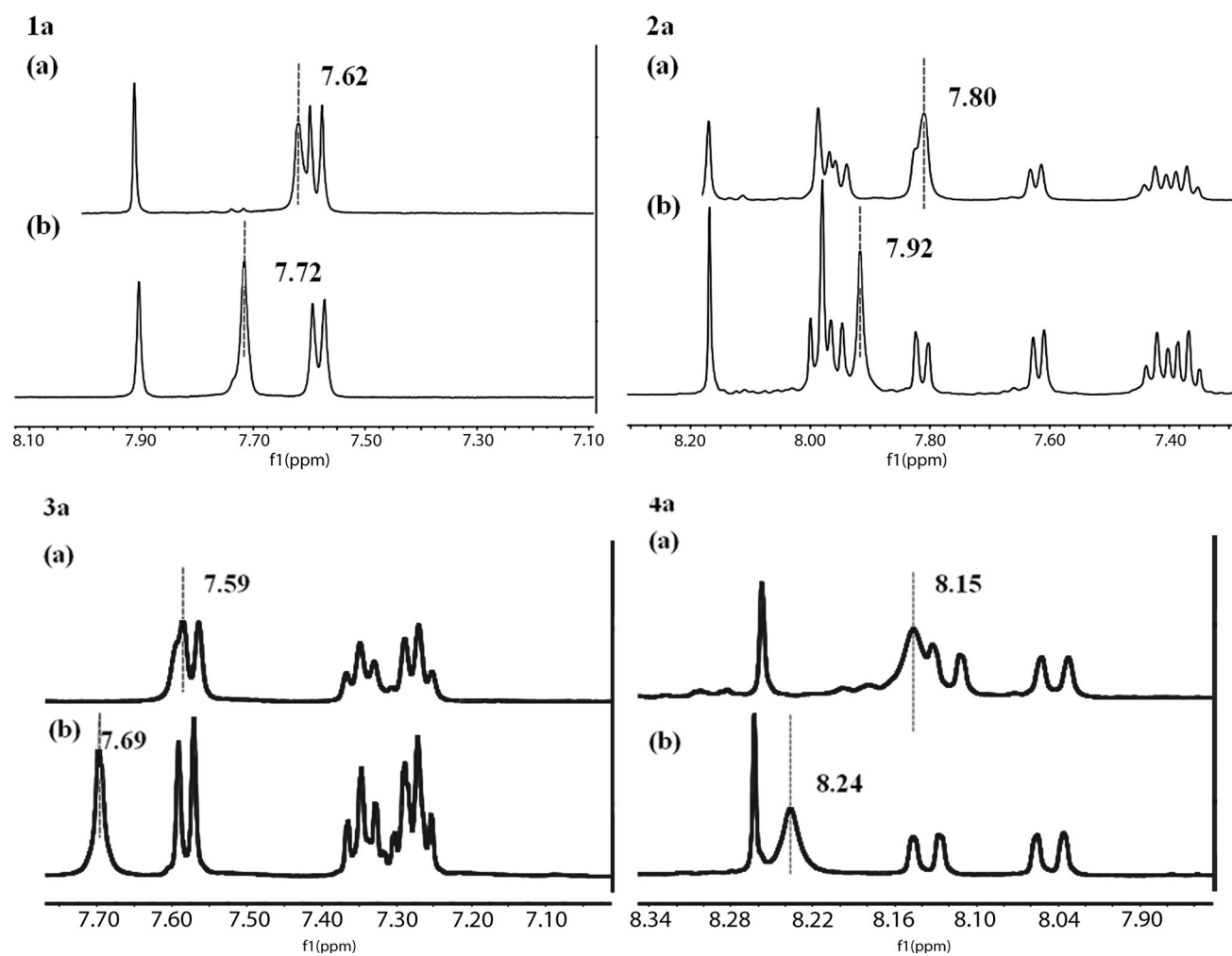
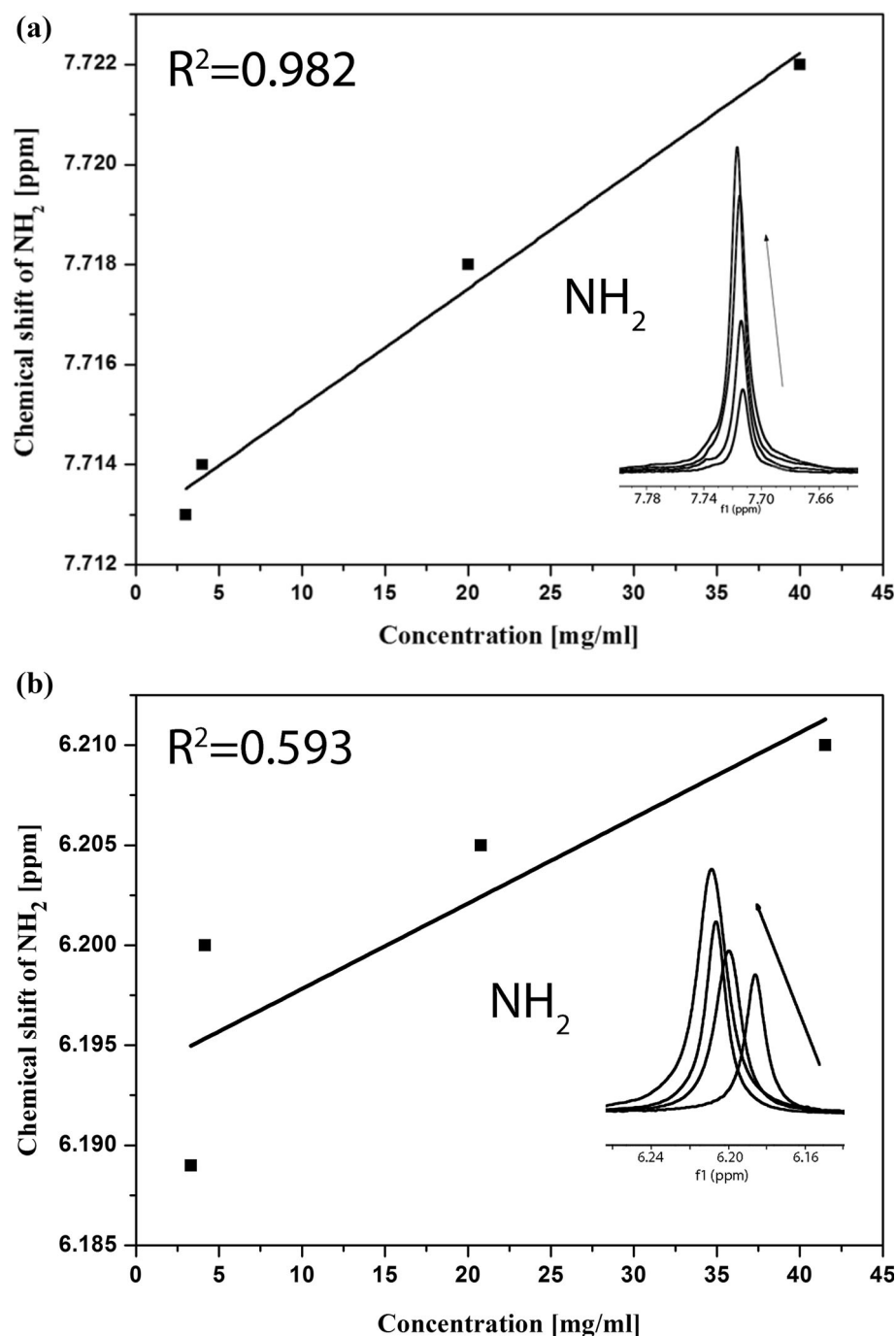


Figure 3 The ^1H NMR spectra registered in $\text{DMSO-}d_6$ of unsymmetrical azomethines **AzTh-1a–AzTh-4a** at **a** 60 °C and **b** 25 °C.

Figure 4 Chemical shifts of the amine protons signal in ^1H NMR spectra of **AzTh-1a** at different concentrations: 0.8, 1, 5 and 10 mM in **a** $\text{DMSO-}d_6$ and **b** CDCl_3 solutions. Insets: NMR spectra of NH_2 signal of **AzTh-1a** with raising concentration.



frequencies due to the decrease in the hydrogen bond strength with increasing temperature was observed (cf. Fig. 3). Next, the effect of concentration of imine **AzTh-1a** in solution on hydrogen bonds formation was investigated. The downfield shift of the amine protons signal with increasing concentration is expected. The chemical shift with an increasing concentration of **AzTh-1a** (from 0.8 to 10 mM) to higher frequencies in two solvents is presented in Fig. 4.

Increasing the concentrations of a sample in solution causes involvement of more protons in hydrogen bond formation, which reduces shielding and hence shifts the proton signals toward higher values of δ , because the protons involved in the hydrogen bond have a much lower electron density [23]. A linear correlation between the chemical shift to higher frequencies together with increasing concentrations was

noticed. This behavior confirms the presence of concentration-induced hydrogen bonding [18].

Thermal properties

Differential scanning calorimetry (DSC) and thermogravimetric analysis (TGA) were applied to define the thermal behavior of the synthesized thiophene azomethines. TGA/DTG and DSC thermograms are presented in Fig. 5, and thermal data are given in Table 1.

Temperatures of 5% (T_5) and 10% (T_{10}) weight loss of azomethines in the range of 221–303 °C and 231–333 °C were recorded, respectively. It was found that symmetrical imines showed better thermal stability considering T_5 than their unsymmetrical analogs (except for **AzTh-2a**).

In DSC thermograms of all imines, registered during the first heating scan, the endotherms due to

melting (T_m) in the temperature range of 170–260 °C were observed (cf. Table 1).

The introduction of the fluorene structure (**AzTh-2a** and **AzTh-2b**) lowered T_m . Similarly to the trend of thermal decomposition, the symmetrical imines melted at higher temperatures compared to the unsymmetrical, with the exception of **AzTh-2a**. Taking into account the DSC thermograms recorded during the second heating run after rapid cooling, it was found that all imines obtained after the reaction as crystalline solids can be converted into amorphous materials with a glass transition temperature (T_g) ranging from 79 to 135 °C. The highest T_g exhibited unsymmetrical imines with pyrrolidone (**AzTh-1a**) and methylindole (**AzTh-3a**) derivatives. The glass transition temperatures for symmetrical **AzTh-1b** and **AzTh-3b** were detected at lower temperatures compared with unsymmetrical counterparts, and the opposite behavior was noticed for **AzTh-2b** and **AzTh-4b** (cf. Table 1). Three symmetrical imines, that

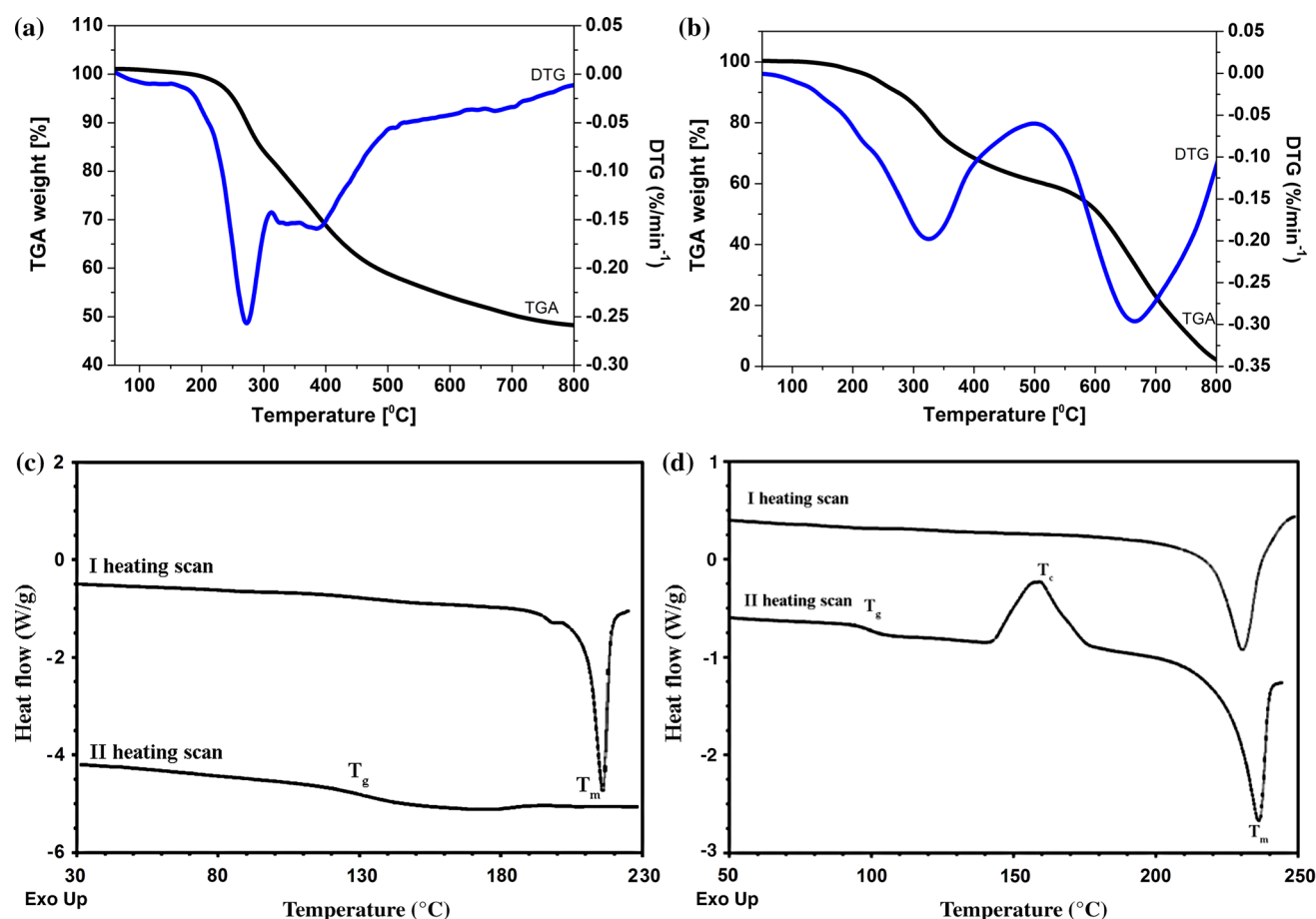


Figure 5 The TGA/DTG thermograms of **a** unsymmetrical **AzTh-2a** and **b** symmetrical **AzTh-2b** azomethine and DSC thermograms of **c** **AzTh-1a** and **d** **AzTh-4b**.

Table 1 Thermal properties of investigated azomethines

Code	TGA			DSC			
				(I run)	(II run)		
	T_5^a (°C)	T_{10}^a (°C)	T_{max}^b (°C)	T_m^c (°C)	T_g^d (°C)	T_c^e (°C)	T_m (°C)
AzTh-1a	221	231	233;316;357	216	135	nd	nd
AzTh-2a	251	273	273;385	184	76	nd	nd
AzTh-3a	221	237	224;337;693	211	122	nd	nd
AzTh-4a	237	268	279;390	216	84	nd	nd
AzTh-1b	265	270	272;409;573	226	79	167	209
AzTh-2b	230	272	330;654	170	90	nd	nd
AzTh-3b	303	333	353;676	260	90	210	253
AzTh-4b	281	310	323	229	99	159	236

nd not detected

^a T_5 , T_{10} —temp. based on 5%, 10% weight loss from TGA curves

^bTemp. of the maximum decomposition rate from DTG curves

^cMelting temp

^dGlass transition temp

^eCrystallization temp

is, bearing pyrrolidine (**AzTh-1b**), methylindole (**AzTh-3**) and benzothiazole (**AzTh-4b**) units, showed a tendency for crystallization. In DSC thermograms of the mentioned molecules, after T_g an exothermic peak due to cold crystallization and next melting endotherm were revealed. The synthesized thiophene azomethines are molecular glasses. The high T_g gives the possibility for preparation of morphologically stable amorphous films.

Redox properties

Redox properties were examined by means of cyclic voltammetry (CV) and differential pulse voltammetry (DPV) as useful methods to determine ionization potentials (IP) and electron affinities (EA). The estimated IP and EA values can be related to the position of the HOMO and LUMO levels, which are important in the design of optoelectronic devices for evaluation of the energy barrier for the injection of holes and electrons. The electrochemical measurements were taken in dichloromethane solution using a platinum coil as a working electrode with 0.1 M Bu_4NPF_6 as an electrolyte. The IP of Fc/Fc^+ was calculated to be equal to -5.1 eV, as shown in literature data [24]. The energy band gap (E_g) based on IP and EA was calculated. Electrochemical data of investigated azomethines are given in Table 2, and the representative voltammograms are depicted in Fig. 6.

Both unsymmetrical and symmetrical azomethines were electrochemically active. The reversible oxidation process was noticed for the azomethines that contained methylindole (**AzTh-3a** $\Delta E = 50$ mV), two *N*-phenylpyrrolidine substituents (**AzTh-1b** $\Delta E = 40$ mV) and *quasi*-reversible for **AzTh-1a** ($\Delta E = 90$ mV). Other compounds undergo irreversible oxidation. The irreversible oxidation of **AzTh-2b** was noticed also by the Skene group [21]. In the case of the reduction process, the $E_{red(onset)}$ in the range of -1.44 to -0.96 V was found, and the lowest potential was found for azomethine **AzTh-4a** with one benzothiazole substituent (cf. Table 2). The imine bond reduction potentials $E_{red -CH=N-}$ measured using the DPV method were in the range of -2.06 to -1.71 V (cf. Table 2) [19, 25]. The lack of the imine bond reduction only for **AzTh-1a** was observed, and it may be related to the fact that this process can occur at higher potentials [16, 21]. In the case of **AzTh-2b**, the Skene group has not observed the reduction of $-CH=N-$; however, the DPV method is more sensitive than the CV method, which could have allowed to detect the reduction process.

Depending on the nature of the substituent attached to the imine bond, either decrease or increase in the cathodic and anodic processes was seen, which resulted in differences in the ionization potentials (IP) and electron affinities (EA) (cf. Table 2). The first reduction and oxidation processes

Table 2 Redox data (vs Fc/Fc⁺), ionization potentials (IP), electron affinities (EA) and the energy band gap (E_g) of presented azomethines

Code	$E_{\text{ox onset}}^{\text{CV}}$ (V)	IP ^{CV} (eV)	$E_{\text{red onset}}^{\text{CV}}$ (V)	$E_{\text{red}}^{\text{DPV}}_{-\text{CH}=\text{N}-}$ (V)	EA ^{CV} (eV)	E_g^{CV} (eV)	HOMO ^{DFT} (eV)	LUMO ^{DFT} (eV)	E_g^{DFT} (eV)
AzTh-1a	0.09 0.05 ^a	- 5.19 - 5.15 ^a	- 1.32 - 1.22 ^a	nd	- 3.78 - 3.88 ^a	1.41 1.27 ^a	- 4.95	- 1.56	3.39
AzTh-2a	0.27 0.33 ^a	- 5.37 - 5.53 ^a	- 1.44 - 1.34 ^a	- 1.71	- 3.66 - 3.76 ^a	1.71 1.77 ^a	- 5.29	- 2.04	3.25
AzTh-3a	0.31 0.23 ^a	- 5.41 - 5.33 ^a	- 1.20 - 1.16 ^a	- 2.06	- 3.90 - 3.94 ^a	1.51 1.39 ^a	- 5.20	- 1.82	3.38
AzTh-4a	0.49 0.42 ^a	- 5.59 - 5.52 ^a	- 1.06 - 0.96 ^a	- 1.73	- 4.04 - 4.14 ^a	1.55 1.38 ^a	- 5.67	- 2.63	3.04
AzTh-1b	0.10 0.06 ^a	- 5.20 - 5.16 ^a	- 1.26 - 1.30 ^a	- 2.04	- 3.84 - 3.80 ^a	1.36 1.36 ^a	- 4.89	- 2.08	2.82
AzTh-2b	0.36 0.32 ^a	- 5.46 - 5.42 ^a	- 1.38 - 1.44 ^a	- 1.72	- 3.72 - 3.66 ^a	1.74 1.76 ^a	- 5.46	- 2.43	3.03
AzTh-3b	0.13 0.04 ^a	- 5.23 - 5.14 ^a	- 1.16 - 1.24 ^a	- 2.00	- 3.94 - 3.86 ^a	1.29 1.28 ^a	- 5.88	- 2.20	2.85
AzTh-4b	0.85 0.91 ^a	- 5.95 - 6.01 ^a	- 1.54 - 1.54 ^a	- 1.74	- 3.56 - 3.56 ^a	2.39 2.45 ^a	- 6.24	- 3.17	3.06

$$\text{IP} = -5.1 - E_{\text{ox onset}}, \text{EA} = -5.1 - E_{\text{red onset}}, E_g^{\text{CV,DPV}} = E_{\text{ox onset}} - E_{\text{red onset}}, E_g^{\text{DFT}} = \text{HOMO-LUMO}$$

nd not detected

^aEstimated by DPV

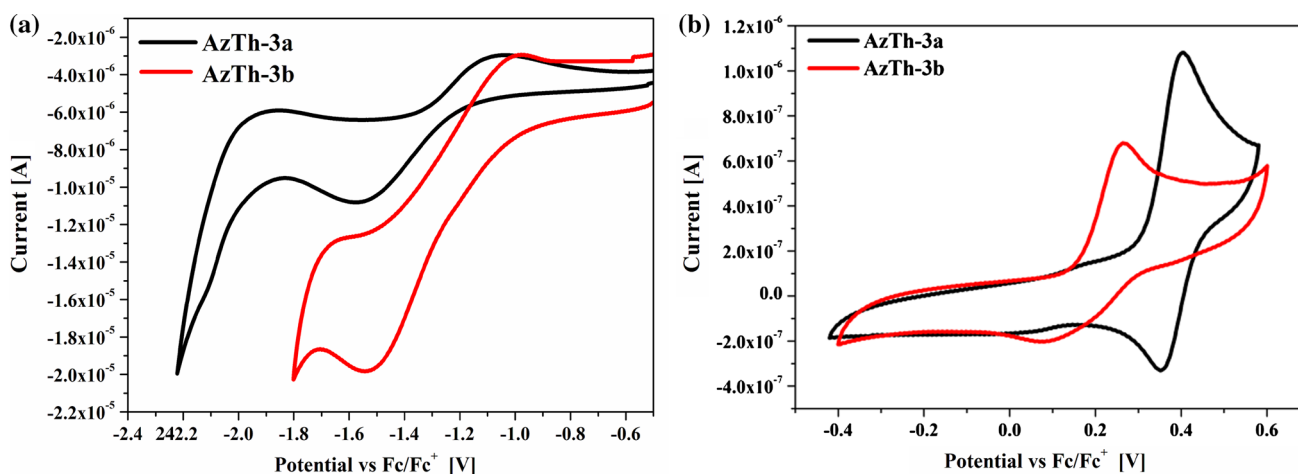


Figure 6 Representative CV voltammograms of **AzTh-3a** and **AzTh-3b**: **a** reduction and **b** oxidation process (Pt as working electrode, $v = 0.100 \text{ V s}^{-1}$, electrolyte 0.1 M Bu₄NPF₆ in dichloromethane).

were probably caused by the reduction of thiophene ring and radicals formation, as was reported previously [21, 24]. The reduction process for symmetrical azomethines occurred at lower potentials, except for **AzTh-4b**, were $E_{\text{red(onset)}} = -1.54 \text{ V}$, and for the unsymmetrical counterpart **AzTh-4a** at $E_{\text{red(onset)}} = -1.06 \text{ V}$. The presence of two benzothiazole substituents (**AzTh-4b**) leads to an increase in the

potential, which indicates that the reduction process is more difficult for this azomethine. The oxidation process for azomethine with one fluorene (**AzTh-2a**) and benzothiazole (**AzTh-4a**) substituents at lower potentials than symmetrical counterparts was observed. This behavior can be caused by the presence of the electron donor group $-\text{NH}_2$; otherwise, similar oxidation potentials for **AzTh-1a** and **AzTh-**

1b were seen (cf. Table 2). In this case, a central part of thiophene probably plays an important role [19]. However, the presence of two *N*-phenylpyrrolidine substituents (**AzTh-1b**) allowed for stabilization of the radical formation and the reversibility of the oxidation process.

The ionization potentials (IP) were obtained in the range from -6.01 to -5.14 eV with the highest value measured for **AzTh-4b** (benzothiazole substituents). The electron affinities (EA) were calculated in the range of -4.14 to -3.56 eV, also with the highest value for **AzTh-4b** (cf. Table 2). The energy band gap (E_g) based on CV results was found to be between 2.39 and 1.29 eV. Nonetheless, except for **AzTh-4b**, the E_g was lower than 2.0 eV (cf. Table 2). Low energy band gaps are beneficial for applications in organic electronics.

Geometric structure and frontier molecular orbitals

The theoretical calculations were performed with the use of the density functional theory (DFT) and were carried out using the Gaussian 09 program. Molecular geometry of the singlet ground state of the compounds was optimized in the gas phase, and its electronic structures, electronic transitions, and first singlet excited states were calculated with the polarizable continuum model (PCM) in chloroform as a solvent. Such calculations were carried out for analysis of the HOMO, LUMO energy levels and UV–Vis and emission data. The optimized structures of the azomethines are depicted in Fig. S1 in Supplementary material (Fig. S2 presents calculated IR spectra). The central thiophene and the substituent rings in unsymmetrical azomethines, except for **AzTh-1a**, are almost planar and the deviation from planarity decreases in series **AzTh-2a** > **AzTh-3a** > **AzTh-4a**. In the case of **AzTh-1a**, the mean plane angle between thiophene and *N*-phenylpyrrolidine is equal to 35.8° . The molecules of the symmetrical azomethines show larger deviation from planarity (cf. Table S3). Based on the optimized geometries, the frontier molecular orbitals of the compounds were analyzed. The contours of HOMO and LUMO are presented in Fig. S5. Comparing the energies of HOMOs and LUMOs determined on the basis of electrochemical data with theoretically obtained (cf. Table 2), it can be seen that calculated HOMO energies are similar to the experimental values of ionization potentials determined

from CV measurements. The large difference of 0.65 eV was observed for **AzTh-3a** compound. On the other hand, calculated LUMO energies are much higher than those determined experimentally. The virtual orbitals are generally harder to be described theoretically than the occupied ones [26]; however, the calculated values of the HOMO and LUMO energies were used only for consistency with geometry optimization. For a more detailed description of the molecular orbitals, the contribution of parts, i.e., thiophene core, imine group, and aromatic substituents fragments to a molecular orbital, were calculated. The obtained DOS diagrams are depicted in Fig. S6, and composition of selected molecular orbitals is given in Table S4 in Supplementary material. For each of these compounds, HOMO and LUMO comprise the whole molecule, although in the asymmetrical azomethines, except the **AzTh-1a**, the thiophene core plays a dominant role in HOMO. LUMO of symmetrical compounds is dominated by π^* orbitals of $-N=CH-R$ fragment. The lower-energy occupied orbitals (H-1, H-2) in both symmetrical and unsymmetrical azomethines are localized on the substituents attached to thiophene via the imine linker.

The compounds are polar in the ground state and in the excited S_1 , S_2 states have dipole moment greater than in the ground state, although in the case of **AzTh-1b** and **AzTh-3b** the change of the dipole moment is small (cf. Table S3).

Spectroscopic properties

The photophysical properties (absorption and emission) of the obtained azomethines were studied in solution and in the solid state. Two solvents, $CHCl_3$ and NMP, with different dielectric constants (ϵ), showing distinct polarity were applied for UV–Vis measurements. UV–Vis and fluorescence (PL) spectra of the azomethines in the solid state as thin films and blends with non-emissive poly(methyl methacrylate) (PMMA) (1 wt% of imine content) were prepared.

The experimental and calculated UV–Vis spectra of the studied imines are given in Fig. 7 and Fig. S7, whereas the spectroscopic parameters are summarized in Table 3.

Generally, the absorption spectra of the studied azomethines consist of two or three absorption bands, in some cases of a pronounced vibrational character. Additionally, the UV–Vis spectra of the

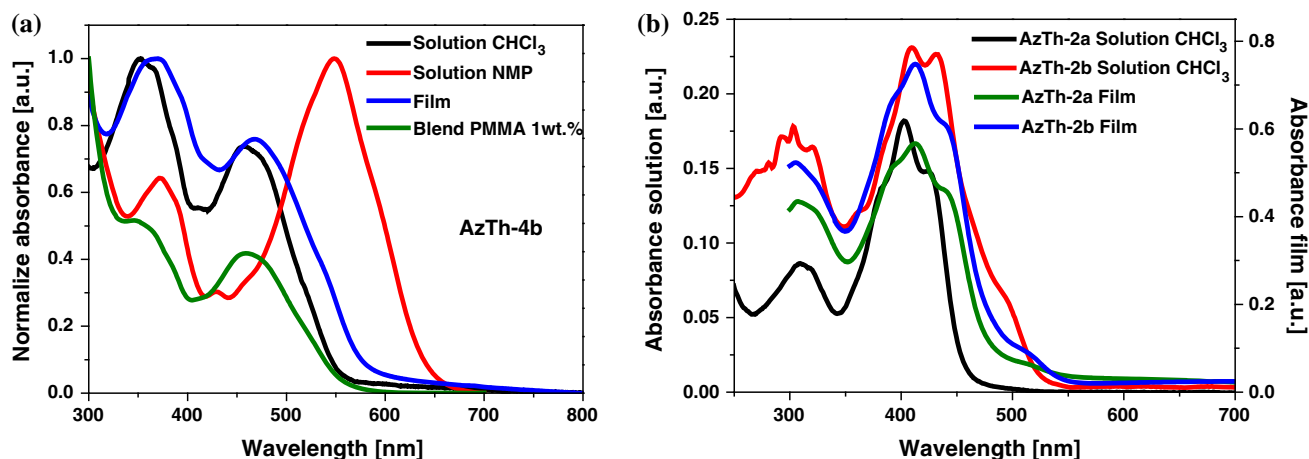


Figure 7 UV-Vis absorption spectra of **a** imine **AzTh-4b** in solutions ($c = 10^{-5} \text{ mol L}^{-1}$), film and blends and **b** symmetrical and unsymmetrical **AzTh-2** in chloroform solution ($c = 10^{-5} \text{ mol L}^{-1}$) and film.

Table 3 UV-Vis electronic data of the imines in solution and in the solid state

Code	Solution		Film	Blend PMMA ^d
	CHCl ₃ ($\epsilon = 4.81$) ^b λ_{max} (nm) ($\epsilon \cdot 10^4$) ^c	NMP ^a ($\epsilon = 33.00$) ^b		
AzTh-1a	330, 416, 433 ^{sh} (2.0, 5.4, 4.7)	319, 420, 440 ^{sh} (2.9, 4.3, 3.7)	332, 371 ^{sh} , 457 ^{sh}	337, 417, 435 ^{sh}
AzTh-2a	309, 383 ^{sh} , 403, 423 (0.8, 1.4, 1.8, 1.5)	309, 412, 434 (1.8, 2.3, 2.1)	300, 394 ^{sh} , 412, 440*	382 ^{sh} , 407, 429*
AzTh-3a	304, 392, 412, 462 (1.1, 1.9, 1.8, 1.1)	277, 357, 467 (2.0, 1.7, 3.0)	425, 482 ^{sh} , 522 ^{sh}	394, 415, 466, 498 ^{sh}
AzTh-4a	305, 442 (2.4, 7.2)	309, 453 (1.4, 4.4)	310*, 437, 462 ^{sh}	429*, 448
AzTh-1b	250, 311, 397, 498 (2.2, 2.1, 3.6, 5.5)	313, 407, 506 (1.8, 3.3, 5.4)	318, 420, 523	396, 446*, 500
AzTh-2b	293, 303, 320, 409, 433 (1.7, 1.8, 1.7, 2.3, 2.9)	312, 411, 434 (3.3, 4.0, 3.7)	305, 390 ^{sh} , 412, 443*, 515 ^{sh}	381 ^{sh} , 407, 430
AzTh-3b	268*, 355, 462 (2.1, 1.7, 2.7)	269, 357, 468 (1.4, 1.8, 3.3)	363*, 430 ^{sh} , 461, 486, 525	349, 463
AzTh-4b	298 ^{sh} , 353, 453 (1.7, 3.0, 2.8)	372, 548 (1.3, 2.0)	301, 370, 468	346, 459

^a $c = 10^{-5} \text{ mol L}^{-1}$

^bDielectric constants

^c ϵ absorption coefficient, [$\text{dm}^3 \text{ mol}^{-1} \text{ cm}^{-1}$]

^d1 wt% concentration of the compound in PMMA

*The second derivatives method was used. ^{sh}shoulder

compounds were calculated with the use of the TD-DFT method (cf. Fig. S7 in Supplementary material). The strong absorption band in the visible region

corresponds to the $S_0 \rightarrow S_1$ transition, while the lower intensity band in the near UV region is connected with $S_0 \rightarrow S_2$ transition. The well-resolved

absorption bands may be due to the large energy gap between the S_2 and S_1 states [27]. According to the TD-DFT calculations, the S_1 state corresponds to the HOMO \rightarrow LUMO, while S_2 to HOMO-1 \rightarrow LUMO transition. Based on the data given in Table S4 and density-of-state (DOS) diagrams shown in Fig. S6, it is visible that main contributions to the HOMO-1 and HOMO come from thiophene and aromatic substituent(s) connected with central core via $-\text{HC}=\text{N}-$. However, the imine linker plays a significant role in LUMO level. Thus, the transitions from HOMO-1/HOMO to LUMO can be followed by charge decrease on the thiophene and substituents and charge increase on the imine part, and thus, the mixed intramolecular charge transfer/locally excited (ICT/LE) nature of S_1 and S_2 states is evident. Considering the fact that in the first excited state, molecules are less planar than in ground state (cf. Table S4), it can

be concluded that ICT takes place in this state. On the other hand, the molecular backbone in S_2 state is more planar than in S_1 and thus in the second excited state prevails LE character. All imines exhibited a solvatochromic effect except for **AzTh-2b** and **AzTh-3a**. The largest bathochromic shift together with the increase in solvent polarity was found for compounds bearing two benzothiazole units (**AzTh-4b**). Symmetrical azomethines with pyrrolidine (**AzTh-1b**) and benzothiazole (**AzTh-4b**) structures showed an absorption band significantly bathochromically shifted compared to their unsymmetrical analogs. The second, weaker intensity, absorption band has smaller solvatochromic shift than the peak in visible region which suggests that S_1 state is more polar than S_2 one. The calculations results presented in Table S3 confirm this conclusion. The electronic spectra of **AzThs** in the film were typically shifted to lower

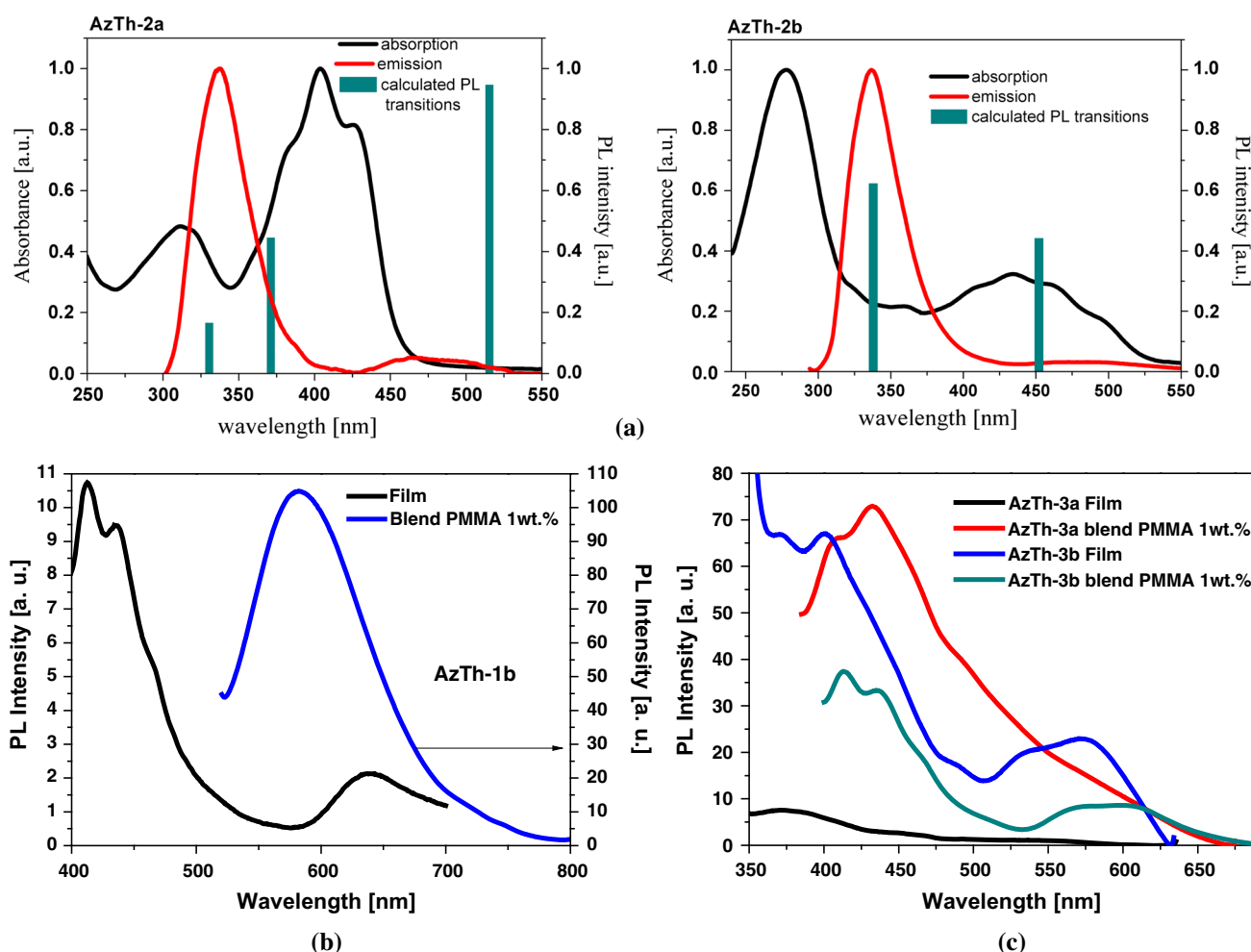


Figure 8 a UV-Vis and PL experimental and calculated spectra of **AzTh-2a** and **AzTh-2b** in chloroform solution, **b** PL spectra of **AzTh-1b** in the solid state and **c** PL spectra of **AzTh-3a** and **AzTh-3b** in film and blend.

Table 4 Fluorescence data of investigated thiophene azomethines

Code	Medium	λ_{ex} (nm)	λ_{em} (nm)
AzTh			
1a	CHCl ₃ ^a	341	380
	Film	320	396
	Blend PMMA ^b	253, 339	372, 390 ^{sh} , 460 ^{sh} , 488
2a	CHCl ₃ ^a	283	338, 464
	Film	320	376, 512
	Blend PMMA ^b	–	–
3a	CHCl ₃ ^a	303	379 ^{sh} , 403, 428 ^{sh}
	Film	325	370
	Blend PMMA ^b	264, 365	404 ^{sh} , 433
4a	CHCl ₃ ^a	279	361 ^{sh} , 381
	Film	320	370, 500
	Blend PMMA ^b	340	370, 491
1b	CHCl ₃ ^a	345	380
	Film	375	412, 436, 430
	Blend PMMA ^b	468, 493	582
2b	CHCl ₃ ^a	284	336, 481
	Film	–	–
	Blend PMMA ^b	270	314, 368 ^{sh} , 485
3b	CHCl ₃ ^a	262	287, 379
	Film	370	413, 436, 599
	Blend PMMA ^b	249, 326	370 ^{sh} , 400, 572
4b	CHCl ₃ ^a	297	344, 363, 380 ^{sh}
	Film	–	–
	Blend PMMA ^b	347	373, 405

– non-emissive

^a $c = 10^{-5}$ mol L⁻¹^b1 wt% concentration of the compound in PMMA

energy with respect to those recorded in solution. Azomethines molecularly dispersed in PMMA (1 wt% content) exhibited similar electronic spectra to the chloroform solution.

The fluorescence spectra of two selected compounds, unsymmetrical **AzTh-1a** and symmetrical **AzTh-1b**, were measured in CHCl₃ and NMP. PL band of imines in NMP solution was significantly shifted from UV to the visible range and quenched compared to the emission observed in chloroform (cf. Fig. S20). Hence, the PL spectra of other imines were registered in CHCl₃ solution. The excitation and emission spectra of all compounds in the chloroform are given in Fig. S21. The representative emission spectra are presented in Fig. 8, and the PL data are given in Table 4.

The imines in chloroform solution emitted when excited in the 279–345 nm region. The solution of azomethines excited with lower energy was non-

emissive. It means that the PL spectra correspond to the S₂ ← S₀ electronic transitions. In the PL spectra of imines with fluorene units (**AzTh-2a** and **AzTh-2b**), two emission bands were seen. The first intense PL band with a maximum emission (λ_{em}) at about 380 nm and the second one, significantly weaker, in a visible range around 480 nm were observed. Thus, they exhibited dual fluorescence at room temperature. Considering the PL intensity, compounds with methylindole (**AzTh-3a** and **AzTh-3b**) were practically non-emissive and weak emission was found also for molecules with benzothiazole structure (**AzTh-4a** and **AzTh-4b**) (cf. Fig. S21). The highest fluorescence quantum yield (Φ_{PL}) of about 2.6 and 8.4% was measured for symmetrical imines bearing pyrrolidone (**AzTh-1b**) and fluorene (**AzTh-2b**), respectively.

To deepen the insight into the excitation states and explanation of PL in chloroform solution and covering the absorption with emission, the DFT calculations were carried out. The fluorescence spectrum of **AzTh-2a** (cf. Fig. 8a and S10) shows two emission bands and more specifically one broad, very weak band with maximum at 464 nm and the second intense band in UV region. The first one originated from S₁ ← S₀ transition, and the second band arises from the S₂ ← S₀ transition. The S₂ ← S₀ fluorescence may appear if the S₂ ← S₁ radiation-less internal conversion process is sufficiently slow. This situation can happen when the energy gap between S₂ and S₁ levels is large enough. It is assumed that the energy gap greater than $\Delta E > 3000$ cm⁻¹ reduces the vibronic coupling between these states and slows the rate of S₂ ← S₁ internal conversion processes [28]. Calculated values of the energy gap between the S₁ and S₂ states given in Table S5 are sufficiently large for the observation of the S₂ emission. In the case of **AzTh-2b**, the energy gap between second and first excited states of 2888 cm⁻¹ indicates the possibility of the conversion process, and the emission bands from S₁ and S₂ states are not separated although the intensity of the long-wave band is definitely lower (cf. Fig. S16). Similar situation occurs for **AzTh-3b** compound. In the case of **AzTh-1b**, the conversion process seems to be definitely easy because the energy difference between the second and first excited states is small (587 cm⁻¹), and therefore, only one emission band that originated from S₁ ← S₀ transition is observed (cf. Fig. S14).

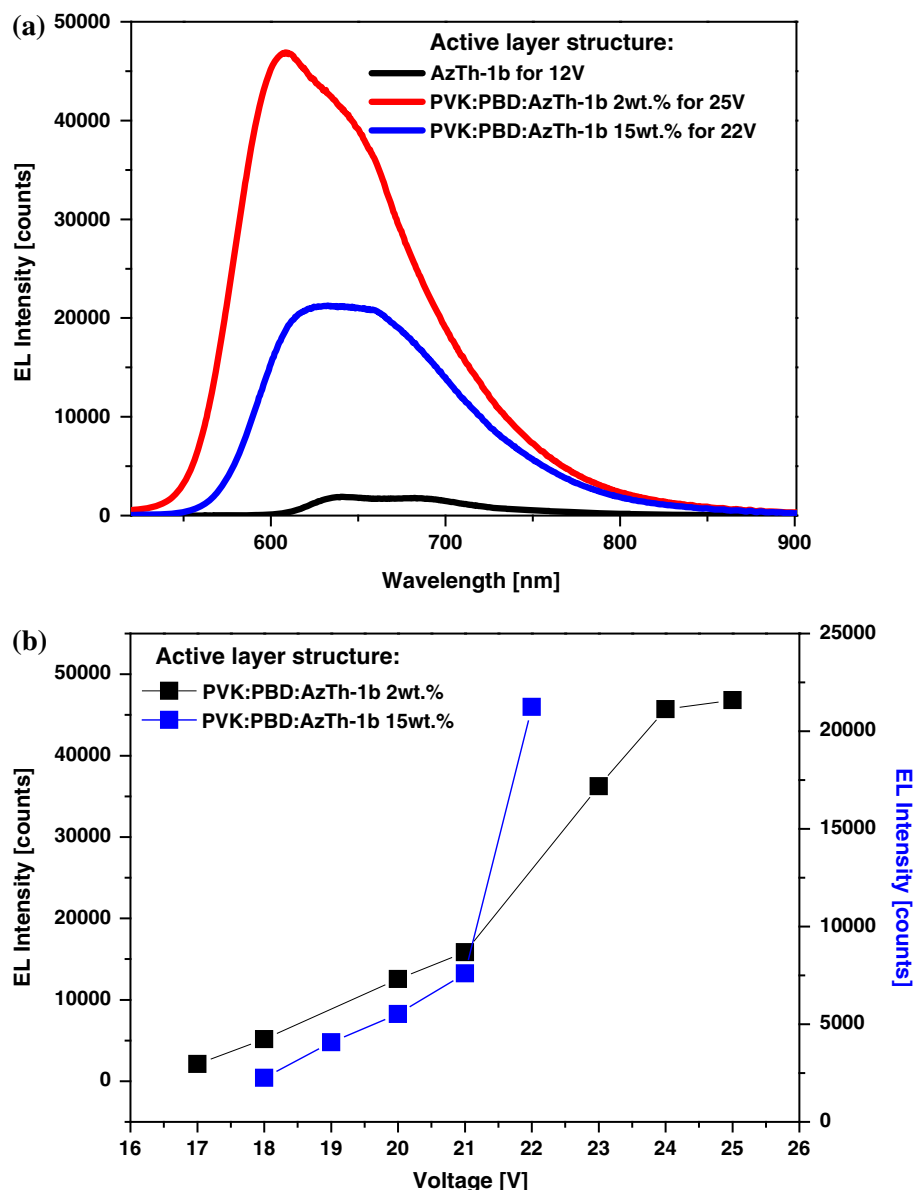


Figure 9 a Electroluminescence spectra of diodes based on **AzTh-1b** and b the relationship between applied voltage and EL intensity.

In the solid state as thin-film imines exhibited weak emission (cf. Fig. 8) except for **AzTh-2b**, and **AzTh-4b**, which were non-emissive due to quenching effect typically observed in solid state [11]. As it was shown, amine groups in unsymmetrical imines can create hydrogen bonds, which should improve the luminescence [18]. It was found that all unsymmetrical imines in film exhibited luminescence, probably due to H-bonds formation.

In order to prevent imine from self-quenching when it is cast as thin film in solid state, the inert polymer PMMA was used as matrix for dispersing

the fluorophore. Thus, compounds were molecularly dispersed (1 wt%) in the polymer matrix. All blends were emissive; however, the most intense emission in the case of **AzTh-1b** and **AzTh-2b**, similar as in chloroform solution, was observed.

Considering the obtained results, for further investigations focused on electroluminescence (EL) ability, one symmetrical imine (**AzTh-1b**), which showed the highest emission in all studied media (solution, film, and blend), was selected. Two kinds of light-emitting diodes with ITO/PEDOT:PSS/**AzTh-1b**/Al and ITO/PEDOT:PSS/PVK:PBD:**AzTh-**

1b/Al structures were constructed. Poly(9-vinylcarbazole) (PVK) and (2-(4-tert-butylphenyl)-5-(4-biphenyl)-1,3,4-oxadiazole) (PBD) were applied as hole- and electron- transporting materials, respectively (PVK:PBD 50:50 in weight %). Diodes with 2 and 15 wt% of imine in a binary matrix were prepared, and their EL spectra were registered (cf. Fig. 9).

All fabricated diodes emitted light in the red range, however with different intensity and position of the maximum emission band (λ_{EL}). In the case of the diode with an active layer consisting of a neat imine, emission of light with $\lambda_{EL} = 640$ and 680 nm was observed. Devices containing imine dispersed molecularly in a PVK:PBD matrix with 2 and 15 wt% content showed λ_{EL} at 609 and 631 nm. The optimal imine content, which gave the most intense EL in the matrix, was 2 wt%. Together with the increase in the external voltage, the increase in emission intensity was found. However, the devices required a rather high value of voltage for the induction of light emission. High turn-on voltages (above 18 V) also showed OLEDs based on imine with thiophene structure reported in our previous work [18]. In turn, lower value of voltage (13 and 14 V) for the light emission exhibited devices bearing in active layer compounds with imine linkages and naphthalimide units [29, 30]. Probably, the presence of a large number of carrier traps makes transport difficult and thus increases the voltage for visible EL. The occurrence of too many carrier traps could cause quenching of the excited state and the reduction in electroluminescence intensity [31]. The utilization of imine with thiophene and phenanthrene moieties in diode with structure ITO/PEDOT:PSS + AgNWs/imine/Al, azomethine with benzofuran unit in device ITO/PEDOT:PSS/10 wt% imine:CBP/TPBI/CsCO₃/Al and imine containing also acetylene linkage in OLED ITO/imine/Au, lowered turn-on voltage to 10, 8 and 5 V, respectively [15, 32, 33].

Conclusions

Summarizing, a series of symmetrical and unsymmetrical thiophene imines were prepared. They were designed and synthesized to investigate the effect of the chemical structure of the substituent conjugated with thiophene ring via azomethine linkages and the presence of terminal amine group on the thermal,

electrochemical, and spectroscopic properties. From the presented results, the following conclusions can be drawn:

- due to the presence of the terminal amine group in unsymmetrical imines, intramolecular hydrogen bonds between $-NH_2$ proton and an oxygen atom from ester group are formed, which was confirmed experimentally and theoretically,
- all azomethines can be converted in amorphous material with high T_g . The symmetrical imines melted at slightly higher temperature about 10°C (except for **AzTh-3**) compared with those of asymmetrical once also without thermal decomposition. The similar relationship concerns T_g . High T_m and T_g of unsymmetrical imines resulted from H-bonds formation,
- the imines showed very low electrochemically estimated E_g value (below 1.74 eV) being in the most cases lower for the symmetrical compounds,
- it was found that the imine linkage plays a role in the excited state and in the emission processes,
- the emission in CHCl₃ of asymmetrical azomethines has $S_2 \leftarrow S_0$ character while in the case of symmetrical compounds the energy difference between second and first excited states allows the internal conversion to the S_1 state,
- the more intense PL with Φ_{PL} 2.6 and 8.4% in solution showed symmetrical imines with pyrrolidone and fluorene derivatives, respectively. However, the imine with fluorene structure was non-emissive in film,
- diodes based on imine containing the fluorene substituents emitted red light.

Electronic supplementary material: The online version of this article (<https://doi.org/10.1007/s10853-019-03853-6>) contains supplementary material, which is available to authorized users.

Acknowledgements

The GAUSSIAN-09 calculations were carried out in the Wrocław Centre for Networking and Supercomputing, WCSS, Wrocław, Poland, <http://www.wcss.wroc.pl> (Grant No. 18).

Open Access This article is distributed under the terms of the Creative Commons Attribution 4.0

International License (<http://creativecommons.org/licenses/by/4.0/>), which permits unrestricted use, distribution, and reproduction in any medium, provided you give appropriate credit to the original author(s) and the source, provide a link to the Creative Commons license, and indicate if changes were made.

Electronic supplementary material: The online version of this article (<https://doi.org/10.1007/s10853-019-03853-6>) contains supplementary material, which is available to authorized users.

References

- [1] Moussallem C, Gohier F, Frère P (2015) Extended benzodifuran-thiophene systems connected with azomethine junctions: synthesis and electronic properties. *Tetrahedron Lett* 56:5116–5119
- [2] Dufresne S, Bourgeaux M, Skene WG (2007) Tunable spectroscopic and electrochemical properties of conjugated push–push, push–pull and pull–pull thiopheno azomethines. *J Mater Chem* 17:1166–1177
- [3] Bolduc A, Dufresne S, Skene WG (2010) EDOT-containing azomethine: an easily prepared electrochemically active material with tuneable colours. *J Mater Chem* 20:4820–4826
- [4] Abbasi AR, Rezvani Z, Nejati K (2006) Synthesis and properties of new liquid crystalline compounds containing an alkoxyphenylazo group. *Dyes Pigments* 70:71–75
- [5] Bolduc A, Al Ouahabi A, Mallet C, Skene WG (2013) Insight into the isoelectronic character of azomethines and vinylenes using representative models: a spectroscopic and electrochemical study. *J Org Chem* 78:9258–9269
- [6] Koole M, Frisenda R, Petrus ML, Perrin ML, van der Zant HSJ, Dingemans TJ (2016) Charge transport through conjugated azomethine-based single molecules for optoelectronic applications. *Org Electron* 34:38–41
- [7] Ng SC, Chan HSO, Wong PML, Tan KL, Tan BTG (1998) Novel heteroarylene polyazomethines: their syntheses and characterizations. *Polymer* 39:4963–4968
- [8] Petrus ML, Bouwer RKM, Lafont U, Athanasopoulos S, Greenham NC, Dingemans TJ (2014) Small-molecule azomethines: organic photovoltaics via Schiff base condensation chemistry. *J Mater Chem A* 2:9474–9477
- [9] Petrus ML, Morgenstern FSF, Sadhanala A, Friend RH, Greenham NC, Dingemans TJ (2015) Device performance of small-molecule azomethines-based bulk heterojunction solar cells. *Chem Mater* 27:2990–2997
- [10] Guarin SAP, Bourgeaux M, Dufresne S, Skene WG (2007) Photophysical, crystallographic and electrochemical characterization of symmetric and unsymmetric self-assembled conjugated thiopheno azomethines. *Org Chem* 72:2631–2643
- [11] Bolduc A, Dufresne S, Skene WG (2012) Chemical doping of EDOT azomethine derivatives: insight into the oxidative and hydrolytic stability. *J Mater Chem* 22:5053–5064
- [12] Bourgeaux M, Skene WG (2007) Photophysics and electrochemistry of conjugated oligothiophene prepared by using azomethine connections. *J Org Chem* 72:8882–8892
- [13] Barik S, Navarathne D, LeBorgne M, Skene WG (2013) Conjugated thiophenoazomethines: electrochromic materials exhibiting visible-to-near-IR color changes. *J Mater Chem* 35:5508–5519
- [14] Al-Janabi OY, Foot PJS, Al-Tikrity ET, Spearman P (2017) Synthesis and characterisation of novel thiophene based azomethine polymers and study of their liquid crystalline, electrochemical and optoelectronic properties. *Polym Polym Compos* 25:345–362
- [15] Kotowicz S, Siwy M, Filapek M, Malecki JG, Smolarek K, Grzelak J, Mackowski S, Slodek A, Schab-Balcerzak E (2017) New donor–acceptor–donor molecules based on quinolone acceptor unit with Schiff base bridge: synthesis and characterization. *J Lumin* 183:458–469
- [16] Dufresne S, Skene WG (2008) Unsymmetric pyrrole, thiophene, and furan-conjugated comonomers prepared using azomethine connections: potential new monomers for alternating homocoupled products. *J Org Chem* 73:3859–3866
- [17] Dufresne S, Bolduc A, Skene WG (2010) Towards materials with reversible oxidation and tuneable colours using heterocyclic conjugated azomethines. *J Mater Chem* 20:4861–4866
- [18] Wałęsa-Chorab M, Tremblay M-H, Skene WG (2016) Hydrogen-bond and supramolecular—contact mediated fluorescence enhancement of electrochromic azomethines. *Chem Eur J* 22:11382–11393
- [19] Kotowicz S, Siwy M, Golba S, Małeckci JG et al (2017) Spectroscopic, electrochemical, thermal properties and electroluminescence ability of new symmetric azomethines with thiophene core. *J Lumin* 192:452–462
- [20] Bourgeaux M, Vomscheid S, Skene WG (2007) Optimized synthesis and simple purification of 2,5-diamino-thiophene-3,4-dicarboxylic acid diethyl ester. *Synth Commun* 37:3551–3558
- [21] Dufresne S, Guarin SAP, Bolduc A, Bourque AN, Skene WG (2009) Conjugated fluorine-thiophenes prepared from azomethine connections Part I. The effect of electronic and aryl groups on the spectroscopic and electrochemical properties. *Photochem Photobiol Sci* 8:796–804

- [22] Joseph PS, Parthasarathi V, Panneerselvan K (1991) Structure of Ethyl 2-Amino-4-phenylthiophene-3-carboxylate. *Acta Cryst* 47:1748–1750
- [23] Grzesiek S, Cordier F, Jaravine V, Barfield M (2004) Insights into biomolecular hydrogen bonds from hydrogen scalar couplings. *Prog Nucl Magn Res SP* 45:275–300
- [24] Bujak P, Kulszewicz-Bajer I, Zagorska M, Maurel V, Wielgus I (2013) Polymers for electronics and spintronics. *Chem Soc Rev* 42:8895–8999
- [25] Bourgeaux M, Skene WG (2007) A highly conjugated p- and n- type polythiopheneazomethine: synthesis, spectroscopic, and electrochemical investigation. *Macromolecules* 40:1792–1795
- [26] Zhang G, Musgrave CB (2007) Comparison of DFT methods for molecular orbital eigenvalue calculations. *J Phys Chem A* 111:1554–1561
- [27] Zhao GJ, Chen RK, Sun MT, Liu JY, Li GY, Gao YL, Han KL, Ch Yang X, Sun L (2008) Photoinduced intramolecular charge transfer and S_2 fluorescence in thiophene- π -conjugated donor-acceptor systems: experimental and TDDFT studies. *Chem Eur J* 14:6935–6947
- [28] Mondal JA, Ghosh HN, Mukherjee T, Palit DK (2005) S_2 fluorescence and ultrafast relaxation dynamics of the S_2 and S_1 states of a ketocyanine dye. *J Phys Chem A* 109:6836–6846
- [29] Kotowicz S, Korzec M, Siwy M, Golba S, Malecki JG, Janeczek H, Mackowski S, Bednarczyk K, Libera M, Schab-Balcerzak E (2018) Novel 1,8-naphthalimides substituted at 3-C position: synthesis and evaluation of thermal, electrochemical and luminescent properties. *Dyes Pigments* 158:65–78
- [30] Gan J-A, Song QL, Hou XY, Chen K, Tian H (2004) 1,8-Naphthalimides for non-doping OLEDs: the tunable emission color from blue, green to red. *J Photochem Photobiol A Chem* 162:399–406
- [31] Geffroy B, Roy P, Prat C (2006) Organic light-emitting diode (OLED) technology: materials, devices and display technologies. *Polym Int* 55:572–582
- [32] Yan L, Li R, Shen W, Qi Z (2018) Multiple-color AIE coumarin-based Schiff bases and potential application in yellow OLEDs. *J Lumin* 194:151–155
- [33] Lim SKJ, Rahamathullah R, Sarih NM, Khairul WM (2018) Tailoring tail-free nematogen of ethynylated-schiff base and its evaluation as solution-processable OLED emitting material. *J Lumin* 201:397–401

Publisher's Note Springer Nature remains neutral with regard to jurisdictional claims in published maps and institutional affiliations.